Supporting Information: Human γS-crystallin copper binding helps buffer against aggregation caused by oxidative damage

Kyle W. Roskamp,[‡] Sana Azim,[§] Günther Kassier,[§] Brenna-Norton Baker,[‡,§] Marc A. Sprague-Piercy,[‖] R. J. Dwyane Miller,[§,⊥] and Rachel W. Martin[*,‡,‖]

‡*Department of Chemistry, University of California, Irvine, CA 92697-2025, USA*

§*Max Planck Institute for the Structure and Dynamics of Matter, Center for Free Electron Laser Science, Luruper Chaussee 149, 22761, Hamburg, Germany.*

‖*Department of Molecular Biology and Biochemistry, University of California, Irvine, CA 92697-3900, USA*

⊥*Department of Chemistry, University of Toronto, Toronto, M5S 3H6, Canada*

E-mail: rwmartin@uci.edu

Running header

Supporting Information:

Human γS-crystallin copper binding helps buffer against aggregation caused by oxidative damage

Table of Contents

Figures:

Tables:

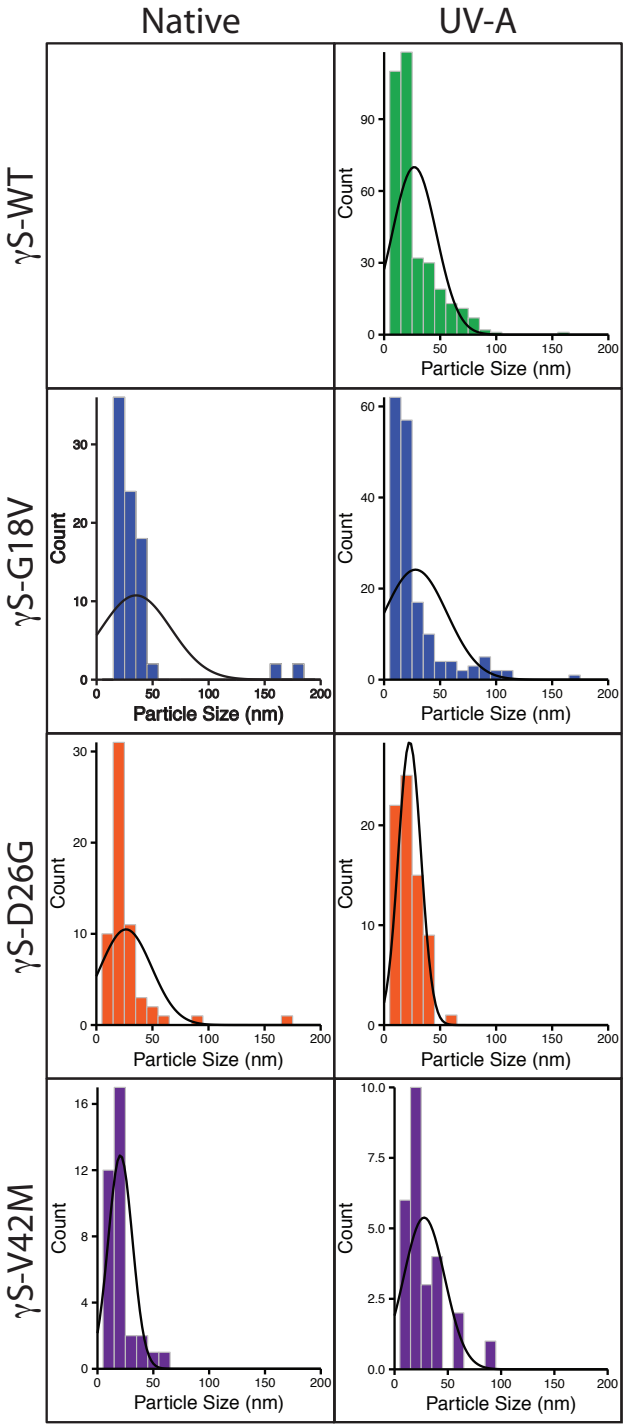

Figure S1: Size distribution histograms for aggregates of γS-crystallin point variants allowed to form without external provocation (left) and those formed through UV-A photodamage (right).

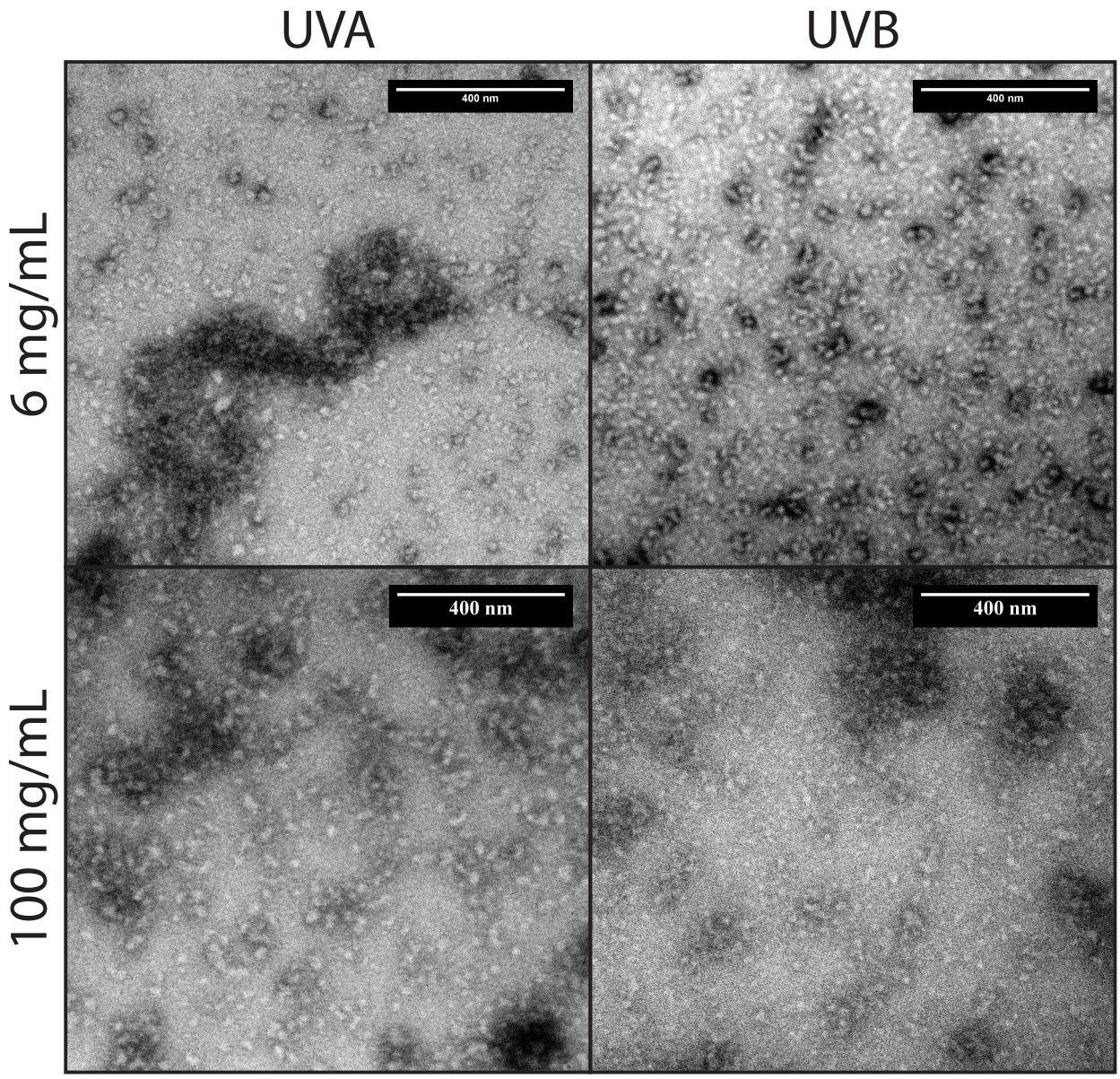

Figure S2: Irradiation of γS-WT from UVA (1.6 kJ/cm^2) and UVB (104.4 J/cm^2) produces aggregates with similar morphology independent of sample concentration during irradiation.

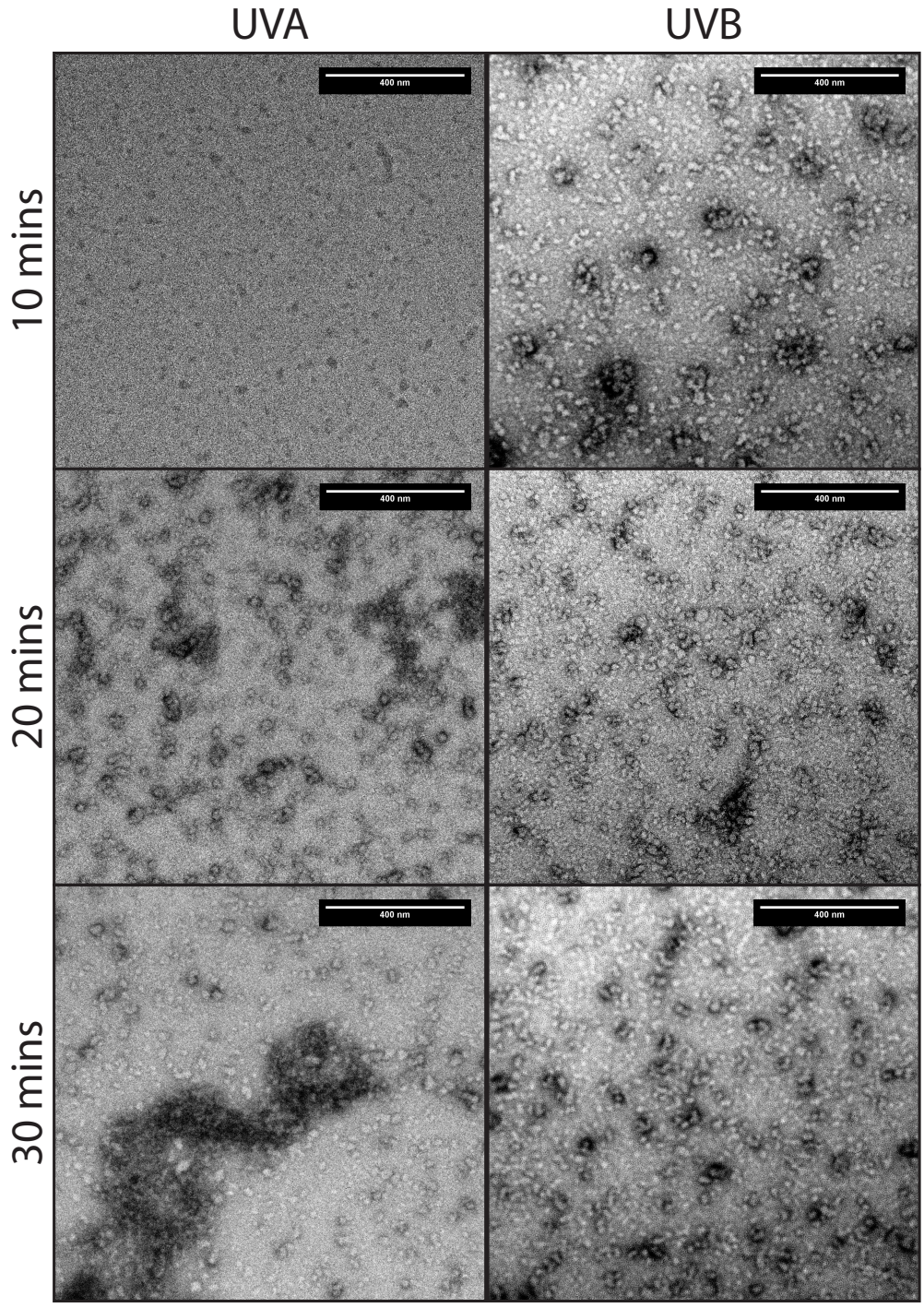

Figure S3: TEM images of aggregates formed from γS-WT after irradiation using UVA or UVB radiation for 10 (0.5 kJ/cm^2, 34.8 J/cm^2), 20 (1.1 kJ/cm^2, 69.6 J/cm^2), and 30 minutes (1.6 kJ/cm^2, 104.4 J/cm^2). Under both treatments, globular aggregates form and these particles associate, yielding larger aggregates.

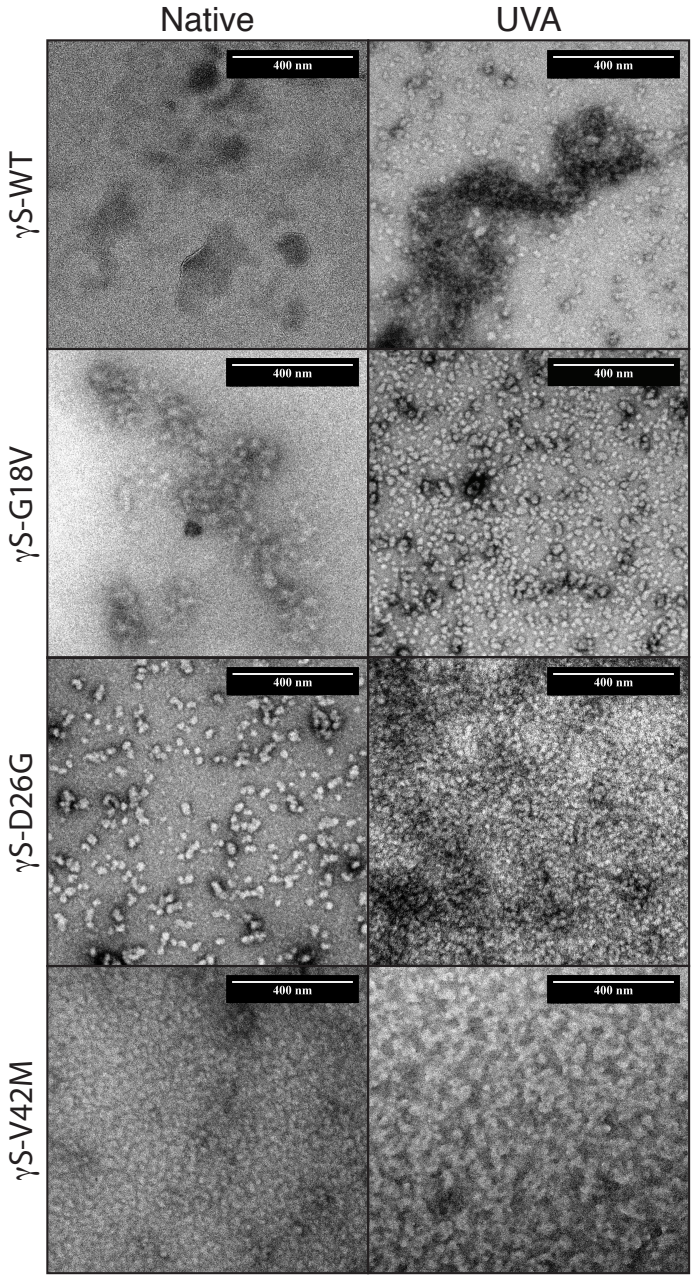

Figure S4: The first panel shows undamaged WT γS-crysallin at the same concentration as for the variants shown in the other images. No aggregates are formed under these conditions. The other panels show TEM images of γS-crystallin aggregates formed either by allowing the sample to precipitate over time as described in the Methods section of the main text, or by irradiation with UVA. Native aggregates from cataract-related point variants are very similar in size and morphology to those formed via UVA photodamage.

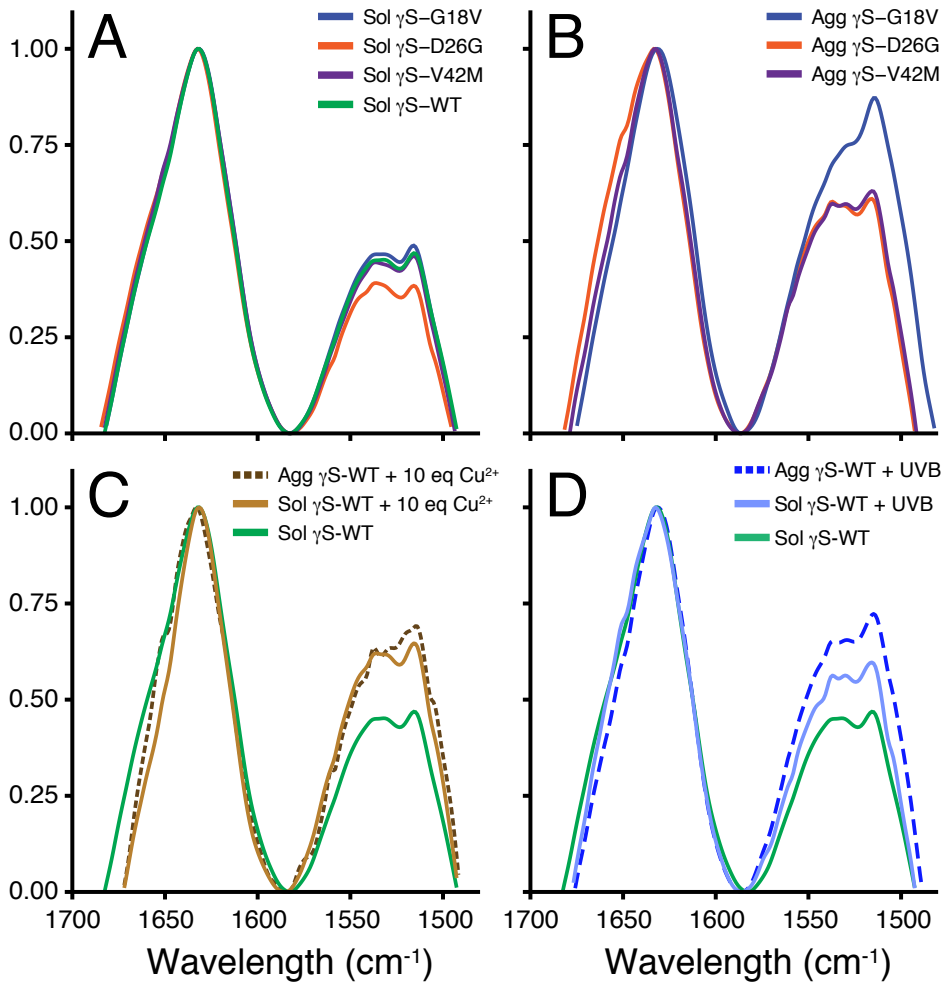

Figure S5: FTIR spectra of aggregated γS-crystallins. (**A**) FTIR of soluble γS-WT and tested point variants exhibit identical spectra. (**B**) Native aggregates of γS point variants exhibit minor broadening of the amide I peak and slightly elevated amide II/I peak intensity ratios. (**C**) Soluble and aggregated γS-WT resulting from $CuCl_2$ treatment show minor narrowing of the amide I peak. As is observed for the γS-crystallin point variants, the amide II/I peak intensity ratio is increased. (**D**) UVB treatment of γS-WT induced similar changes to $CuCl_2$ treatment for soluble and insoluble species.

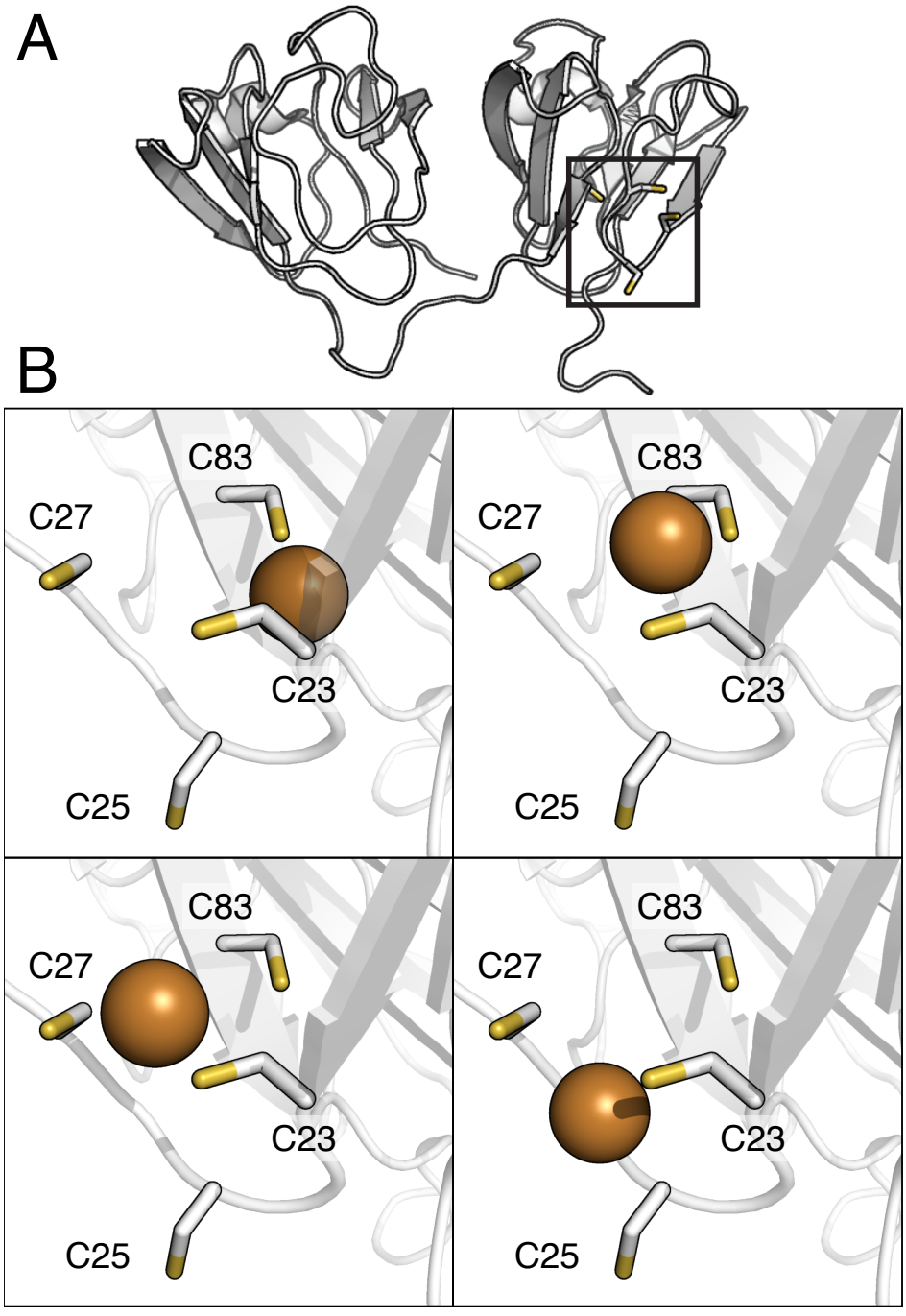

Figure S6: **(A)** Structure of human γS-crystallin (PDBID: 2M3T[1]), with the location of the cysteine loop indicated by an open rectangle. **(B)** Predicted Cu^{+} binding sites for γS-crystallin generated via the MIB webserver (http://bioinfo.cmu.edu.tw/MIB/).[2,3] Binding predictions implicated some or all of C23, C25, C27, and C83 in the majority of the results.

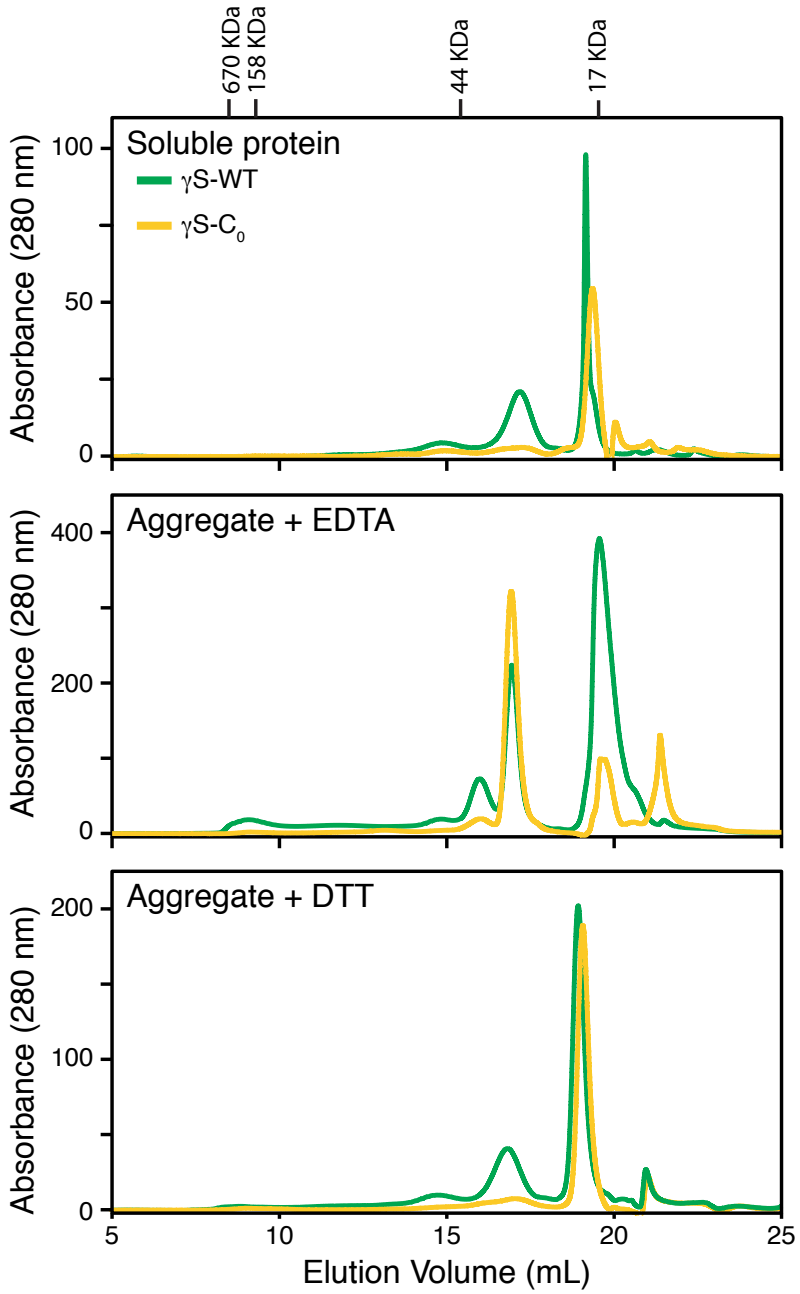

Figure S7: Analytical SEC measurements for γS-WT and γS-C_0 collected separately following Cu^{2+} treatment. The soluble sample (top panel) was collected as the supernatant following treatment. The aggregates that were resuspended during the subsequent EDTA treatment were then collected (middle panel). Finally, the remaining aggregates were treated with DTT, with the resulting resuspension collection as the final samples. (bottom panel). Prior to loading onto the SEC, each sample was treated with EDTA and DTT in order to minimize potential damage to the column. The distribution of protein species for γS-WT is similar across the three chromatograms. Monomers compose the bulk of the elutants while a dimer peak is also clearly observable. In contrast to γS-WT, in γS-C_0, monomeric species are almost exclusively present in the remaining soluble and DTT-resolubilized chromatograms. The EDTA-resolubilized chromatogram of γS-C_0 is primarily dimeric with a low level of monomer present.

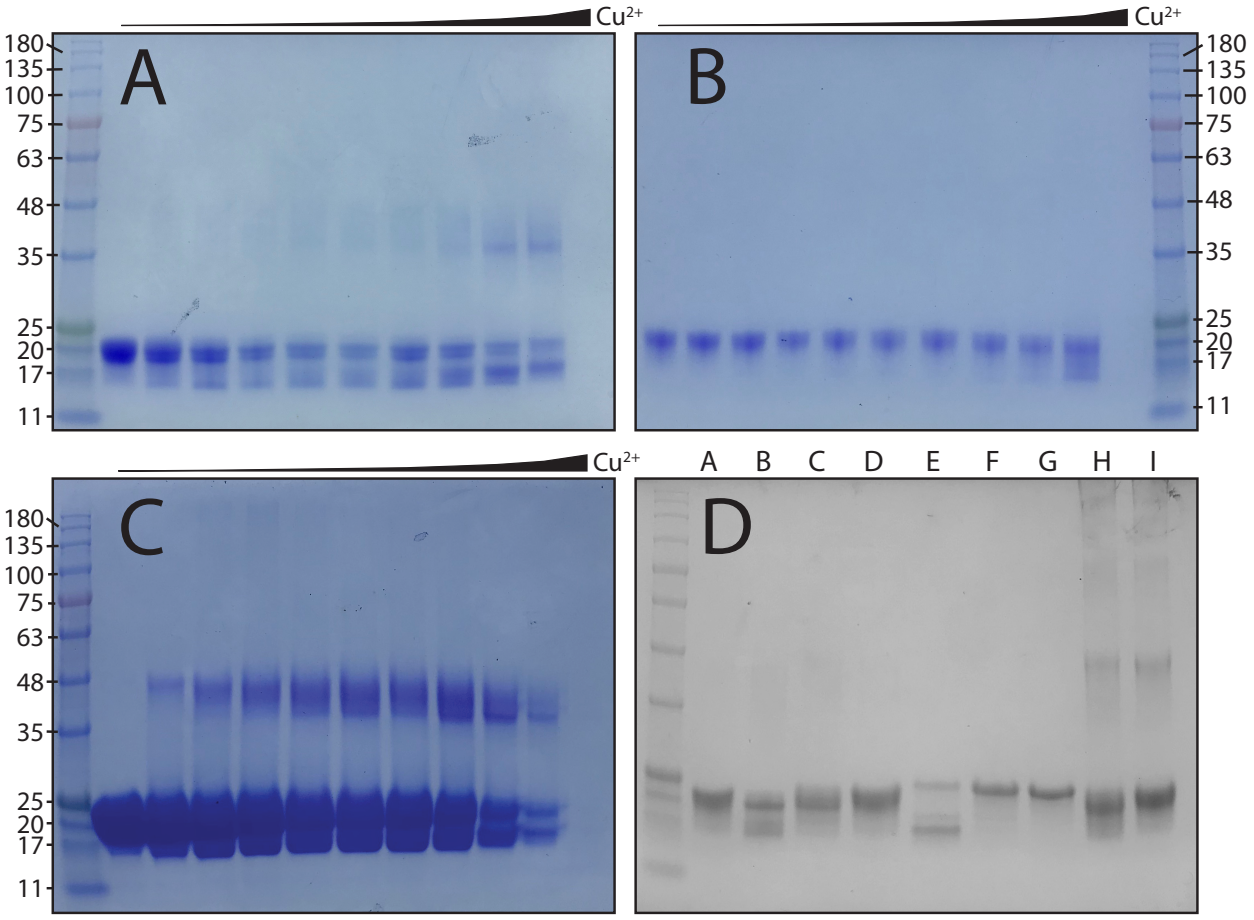

Figure S8: SDS-PAGE separation of γS-crystallin species after treatment with $CuCl_2$. The gradient (left to right) used for all gels was 0, 0.1, 0.2, 0.4, 0.6, 0.8, 1, 1.5, 2, 3, and 5 equivalents of $CuCl_2$. The lanes of gels A and B were loaded with equal concentrations and volumes of protein, with the exception of the 5 equivalents lane, for which only trace amounts of protein remained soluble. For gel C the samples were prepared with equal volumes of the remaining soluble protein such that the observed loss of protein is representative of the increased insoluble fraction. (**Gel A**) Soluble γS-WT after incubation with increasing levels of $CuCl_2$. (**Gel B**) Soluble γS-WT after incubation with increasing levels of $CuCl_2$ and reduction subsequent reduction with BME. (**Gel C**) Soluble γS-WT after incubation with increasing levels of of $CuCl_2$. (**Gel D**) A: γS-WT, B-D: γS-WT treated 1 equiv $CuCl_2$ alone (B), with EDTA (C), with EDTA and BME (D), E-G: γS-C_0 treated 1 equiv $CuCl_2$ alone (E), with EDTA (F), or with EDTA and BME (G), H: soluble UV-B treated γS, I: soluble UV-B treated γS with BME.

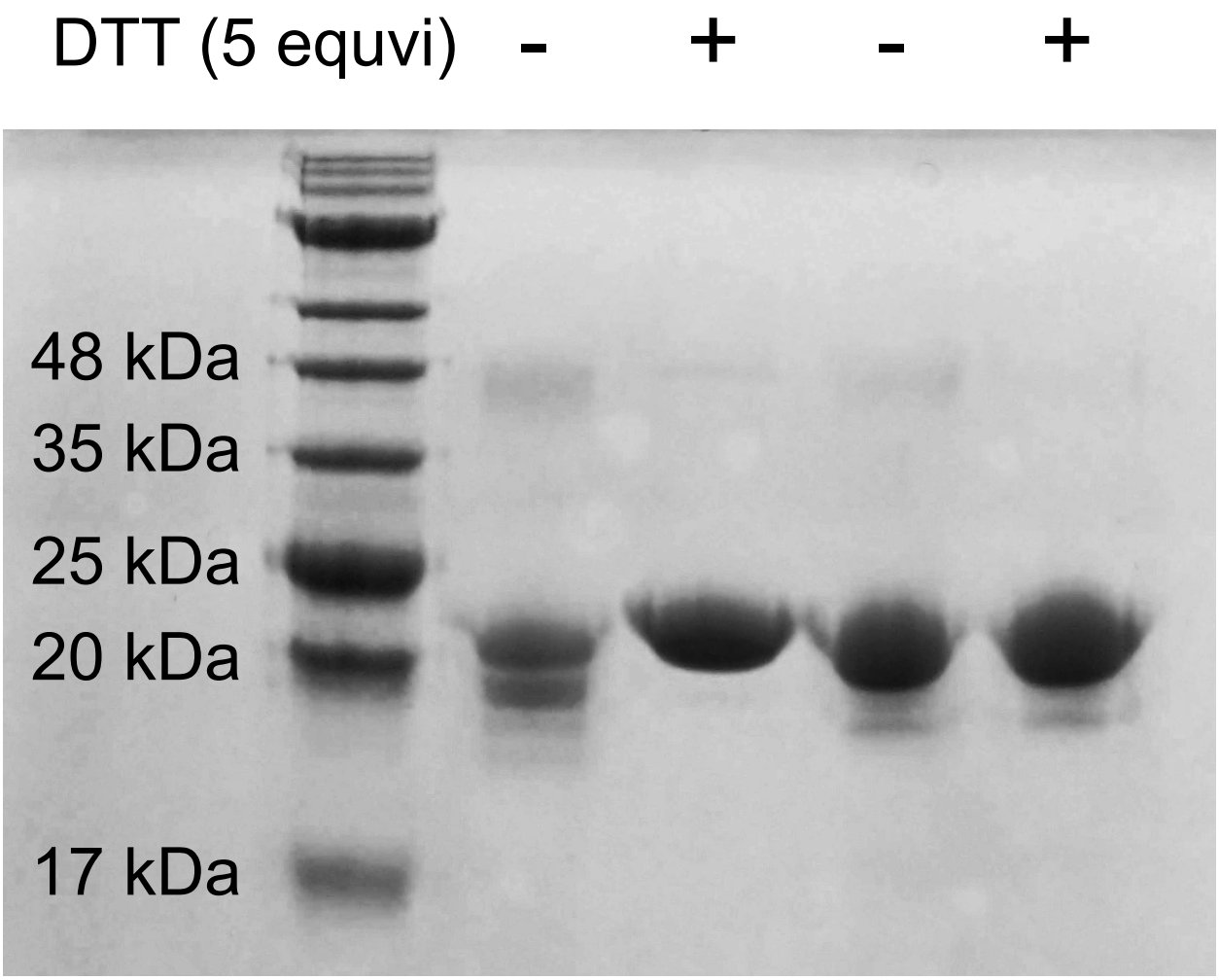

Figure S9: SDS-PAGE analysis of γS-WT stored for 5 months. Two independent samples were stored at 10 mg/mL in the absence of reducing agent at 4 °C for 5 months. Prior to electrophoresis, lanes 2 and 4 were treated with 5 equivalents of DTT. The first two lanes show that the intramolecular disulfide bonds formed are completely reducible, whereas the intramolecular disulfide formed in lane 3 shows negligible reduction following DTT treatment (lane 4). In both cases, the low levels of dimeric species observed are eliminated following reduction.

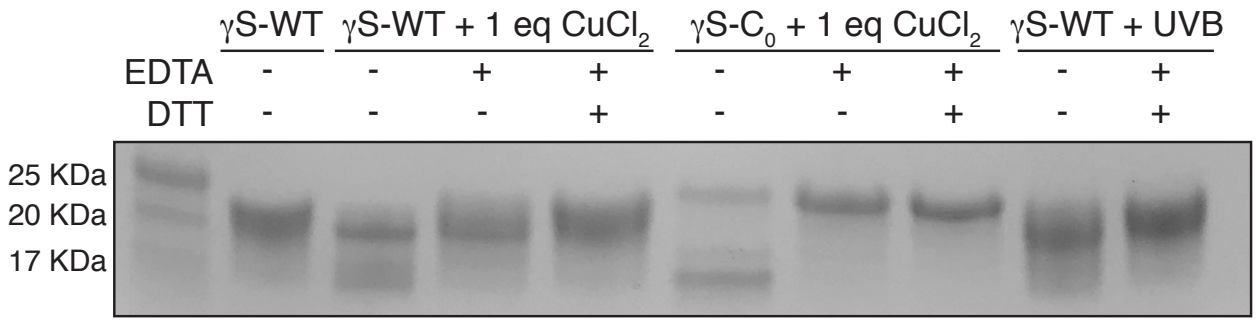

Figure S10: SDS-PAGE analysis of chelating agent-treated γS-crystallin aggregates. Lanes are labeled from left to right, following the ladded.. Lane 1: γS-WT, Lane 2: γS-WT treated 1 equiv $CuCl_2$ alone, Lane 3: sample 2 with EDTA, Lane 4: sample 2 with EDTA and BME, Lane 5: γS-C_0 treated 1 equiv $CuCl_2$, Lane 6: sample 5 with EDTA, Lane 7: sample 5 with EDTA and BME, Lane 8: soluble UV-B-treated γS-WT, Lane 9: sample 7 with BME.

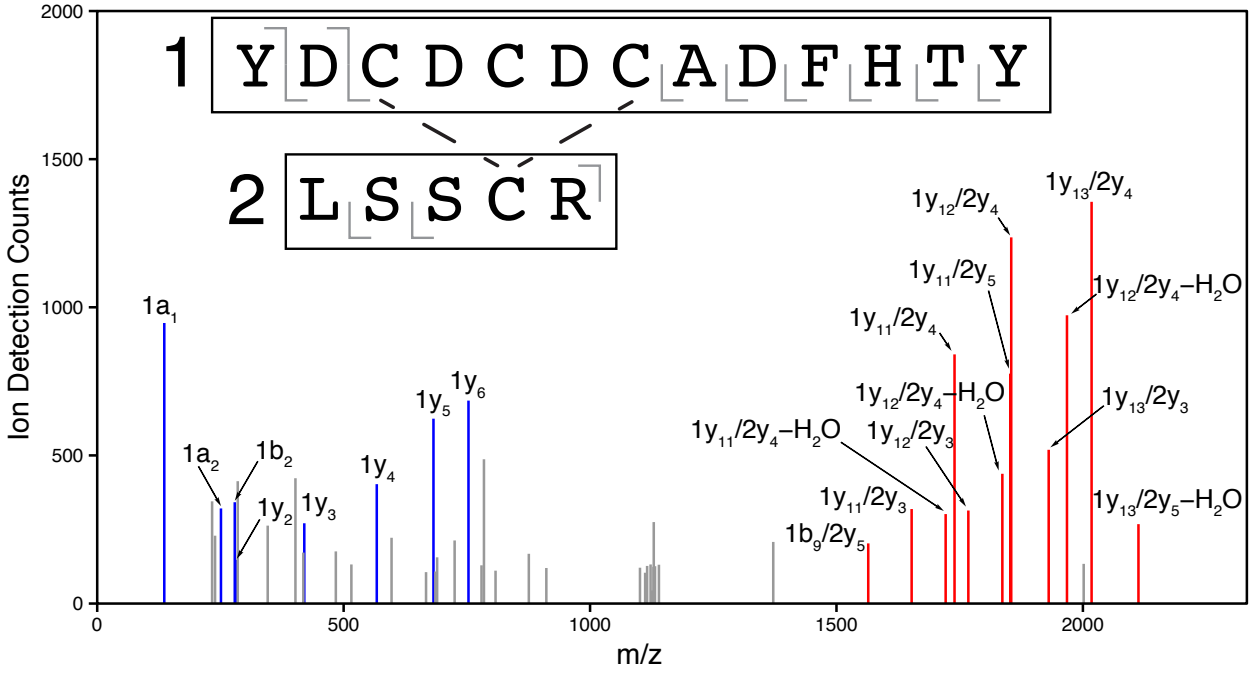

Figure S11: The observed secondary fragmentation observed for the YDCDCDCADFHTY/LSSCR peptides containing an intramolecular disulfide bond. Fragments containing the intramolecular disulfide bond are colored red, while fragments of only one of the peptides are colored blue. The first peptide, YDCDCDCADFHTY, and second peptide, LSSCR, are indicated by the numbers '1' and '2', respectively. A slash between fragments indicates an intramolecular disulfide bond. The observed masses for each fragment are listed in Table S1.

Table S1: MS-MS fragmentation of disulfide-bonded YDCDCDCADFHTY and LSSCR peptides

Peptide	**Assignment**	**Fragment Mass (Da)**	**Control Peak Mass (Da)**	**Intensity (counts)**
YDCDCDCADFHTY/LSSCR	$1y_{13}/2y_5$	2130.7302	2130.7053	9900
YDCDCDCADFHTY/LSSCR - H_2O	$1y_{13}/2y_5$-H_2O	2112.7197	2112.6934	268
YDCDCDCADFHTY/SSCR	$1y_{13}/2y_4$	2017.6461	2017.6318	1356
DCDCDCADFHTY/SSCR	$1y_{12}/2y_4$-H_2O	1967.6669	1967.6307	973
YDCDCDCADFHTY/SCR	$1y_{13}/2y_3$	1930.6141	1930.5786	519
DCDCDCADFHTY/SSCR	$1y_{12}/2y_4$	1854.5828	1854.5564	1236
CDCDCADFHTY/LSSCR	$1y_{11}/2y_5$	1852.6399	1852.6012	776
DCDCDCADFHTY/SSCR	$1y_{12}/2y_4$-H_2O	1836.5723	1836.5405	438
DCDCDCADFHTY/SCR	$1y_{12}/2y_3$	1767.5508	1767.5309	314
CDCDCADFHTY/SSCR	$1y_{11}/2y_4$	1739.5558	1739.5308	841
CDCDCADFHTY/SSCR - H_2O	$1y_{11}/2y_4$-H_2O	1721.5453	1721.5142	302
CDCDCADFHTY/SCR	$1y_{11}/2y_3$	1652.5238	1652.4958	319
ADFHTY	$1y_6$	753.3207	753.3135	685
DFHTY	$1y_5$	682.2836	682.2804	624
FHTY	$1y_4$	567.2567	567.2583	403
HTY	$1y_3$	420.1883	420.1905	271
TY	$1y_2$	283.1294	283.1385	148
YD	$1b_2$	279.0981	279.1046	342
YD	$1a_2$	251.1032	251.1118	321
Y	$1a_1$	136.0762	136.0835	947

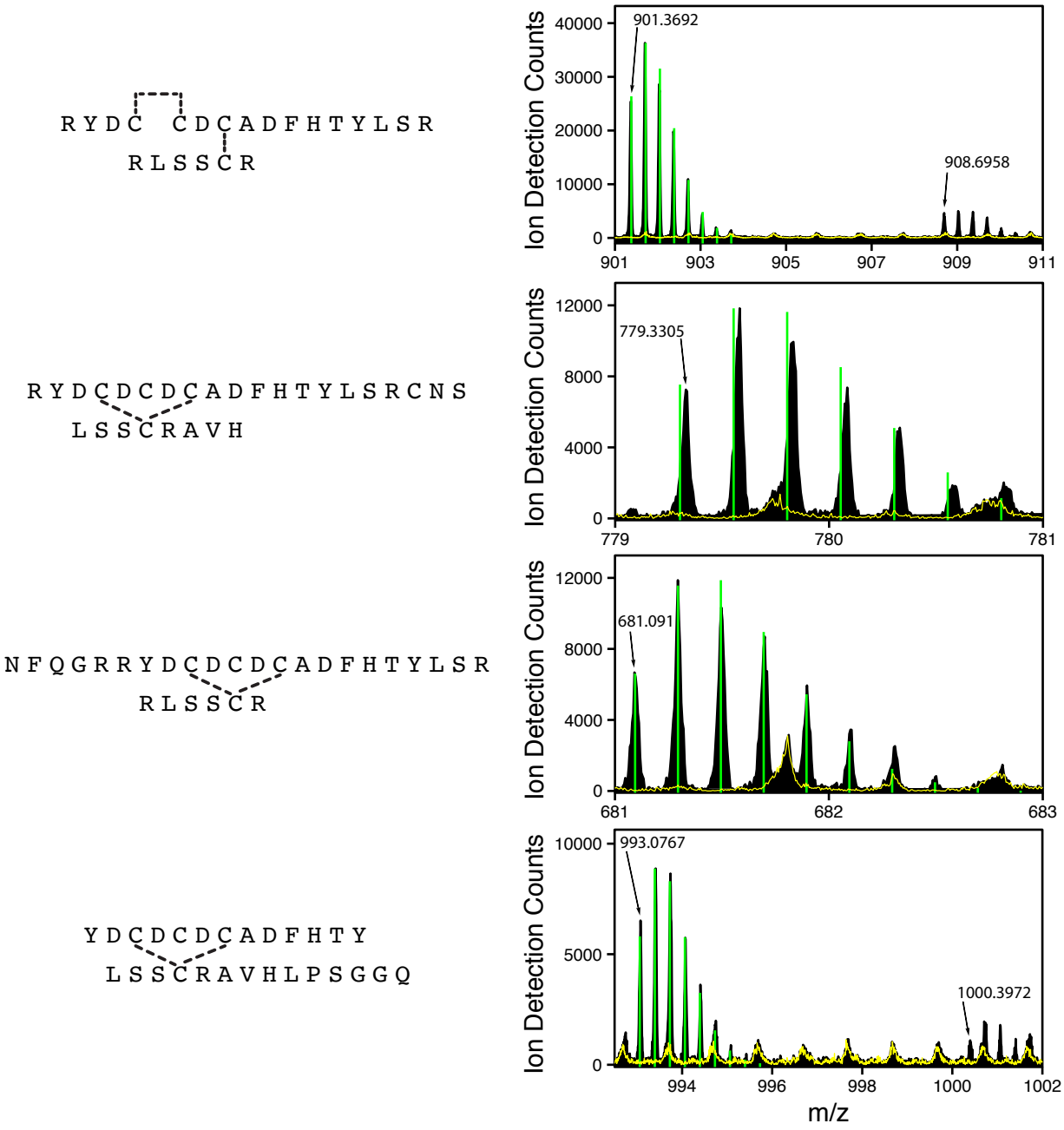

Figure S12: Digested fragments containing an intramolecular disulfide bond were identified by their disappearance following the addition of DTT. The peptide trace without DTT is colored black and the peptide trace with DTT is colored yellow. The predicted isotope pattern for the fragment is shown as green bars. Secondary fragmentation was not sufficient to confirm the location of the intramolecular disulfides were between peptides. The Na^+-bound versions of fragments 1 and 4 were also observed and are shown in the respective traces.

Table S2: Cysteine content of human α-, β-, and γ-crystallins

Protein	**No. Residues**	**No. Cysteines**	**Percentage Cysteine**	**UniProt ID**
αA	173	2	1.16%	CRYAA_HUMAN
αB	175	0	0.00%	CRYAB_HUMAN
βA1*	198	5	2.53%	CRBA1_HUMAN
βA2	197	6	3.05%	CRBA2_HUMAN
βA3	215	5	2.33%	CRBA1_HUMAN
βA4	196	5	2.55%	CRBA4_HUMAN
βB1	252	1	0.40%	CRBB1_HUMAN
βB2	205	2	0.98%	CRBB2_HUMAN
βB3	211	2	0.95%	CRBB3_HUMAN
γA	174	9	5.17%	CRGA_HUMAN
γB	175	7	4.00%	CRGB_HUMAN
γC	174	8	4.60%	CRGC_HUMAN
γD	174	6	3.45%	CRGD_HUMAN
γS	178	7	3.93%	CRGS_HUMAN

*Note: βA1 is an isoform of βA3 generated via an alternate translation initiation site

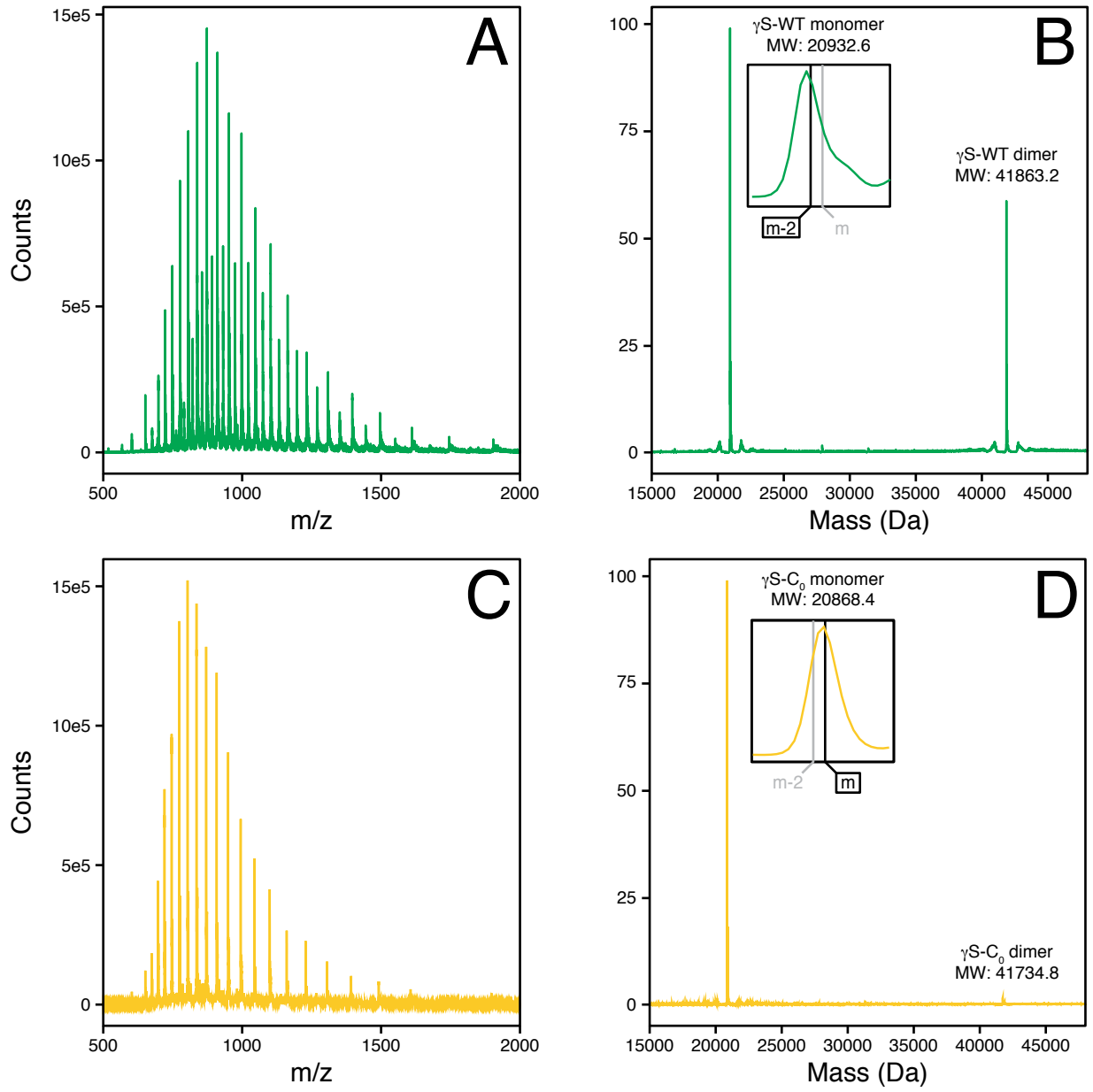

Figure S13: The mass spectra and reconstructed masses for soluble fractions of γS-WT (A, B) and γS-C_0 (C,D) following incubation with 2 equivalents of Cu^{2+}. Dimeric species are evidenced as a doubly-charged species in the raw mass spectrum of γS-WT and the resulting mass reconstruction. In contrast, minimal levels of dimer are observed for γS-C_0. The expected monomeric and dimeric molecular weights are shown for γS-WT and γS-C_0 in panels C and D. The dimer masses assume a singular intermolecular disulfide bond. Inset images show the mass reconstruction for the monomeric peak. The observed mass for γS-WT is consistent with an m-2 species, while the mass of the γS-C_0 peak is consistent with the expected mass (m).

References

(1) Brubaker, W. D., and Martin, R. W. (2012) 1 H, 13 C, and 15 N assignments of wild-type human γS-crystallin and its cataract-related variant γS-G18V. *Biomol. NMR Assign. 6*, 63–67.

(2) Lu, C.-H., Lin, Y.-F., Lin, J.-J., and Yu, C.-S. (2012) Prediction of metal ion–binding sites in proteins using the fragment transformation method. *PloS One 7*, e39252.

(3) Lin, Y.-F., Cheng, C.-W., Shih, C.-S., Hwang, J.-K., Yu, C.-S., and Lu, C.-H. (2016) MIB: metal ion-binding site prediction and docking server. *J. Chem. Inf. Model. 56*, 2287–2291.